

Diffuse optical imaging of brain activation: approaches to optimizing image sensitivity, resolution, and accuracy

David A. Boas,* Anders M. Dale, and Maria Angela Franceschini

Anthinoula A. Martinos Center for Biomedical Imaging, Massachusetts General Hospital, Harvard Medical School, Charlestown, MA 02129, United States

Available online 11 September 2004

Near-infrared spectroscopy (NIRS) and diffuse optical imaging (DOI) are finding widespread application in the study of human brain activation, motivating further application-specific development of the technology. NIRS and DOI offer the potential to quantify changes in deoxyhemoglobin (HbR) and total hemoglobin (HbT) concentration, thus enabling distinction of oxygen consumption and blood flow changes during brain activation. While the techniques implemented presently provide important results for cognition and the neurosciences through their relative measures of HbR and HbT concentrations, there is much to be done to improve sensitivity, accuracy, and resolution. In this paper, we review the advances currently being made and issues to consider for improving optical image quality. These include the optimal selection of wavelengths to minimize random and systematic error propagation in the calculation of the hemoglobin concentrations, the filtering of systemic physiological signal clutter to improve sensitivity to the hemodynamic response to brain activation, the implementation of overlapping measurements to improve image spatial resolution and uniformity, and the utilization of spatial prior information from structural and functional MRI to reduce DOI partial volume error and improve image quantitative accuracy.

© 2004 Elsevier Inc. All rights reserved.

Keywords: Near-infrared spectroscopy; Diffuse optical imaging; HbR; HbT

Introduction

Near-infrared spectroscopy (NIRS) and diffuse optical imaging (DOI) are emerging techniques used to study neural activity in the human brain. DOI employs safe levels of optical radiation in the wavelength region 650–950 nm, where the relatively low attenuation of light accounts for an optical penetration through several centimeters of tissue. As a result, it is possible to noninvasively probe the human cerebral cortex using near-infrared light and to monitor the cerebral concentration of hemoglobin, which is the dominant near-infrared absorbing species in the brain. Furthermore, the difference in the near-infrared absorption spectra

of oxyhemoglobin (HbO₂) and deoxyhemoglobin (HbR) allows the separate measurement of the concentrations of these two species. To achieve this goal, it is sufficient to perform NIRS measurements at two wavelengths. The sum of the concentrations of oxy- and deoxyhemoglobin provides a measure of the cerebral blood volume (CBV), while the individual concentrations of the two forms of hemoglobin are the result of the interplay between physiological parameters such as regional blood volume, blood flow, and metabolic rate of oxygen consumption. NIRS thus offers an advantage over BOLD-fMRI which cannot disentangle blood flow and oxygen consumption changes without also acquiring blood flow images (Davis et al., 1998; Hoge et al., 1999). This ability is potentially important for a wide range of brain studies particularly of the developing and diseased brain. Extension of a spectroscopic measurement in a single location to include a large number of sources and detectors enables reconstruction of diffuse optical images of a large area of the brain.

Since the mid-1990s, an increasing number of researchers have used near-infrared spectroscopy and diffuse optical imaging for human functional brain studies. They have employed the technique to study cerebral response to visual (Heekeren et al., 1997; Meek et al., 1995; Ruben et al., 1997), auditory (Sakatani et al., 1999), and somatosensory (Franceschini et al., 2003; Obrig et al., 1996) stimuli; other areas of investigation have included the motor system (Colier et al., 1999; Hirth et al., 1996; Kleinschmidt et al., 1996) and language (Sato et al., 1999). Still other researchers have addressed the prevention and treatment of seizures (Adelson et al., 1999; Sokol et al., 2000; Steinhoff et al., 1996; Watanabe et al., 2000) and psychiatric concerns such as depression (Eschweiler et al., 2000; Matsuo et al., 2000; Okada et al., 1996b), Alzheimer disease (Fallgatter et al., 1997; Hanlon et al., 1999; Hock et al., 1996), and schizophrenia (Fallgatter and Strik, 2000; Okada et al., 1994), as well as stroke rehabilitation (Chen et al., 2000; Nemoto et al., 2000; Saitou et al., 2000; Vernieri et al., 1999).

While NIRS and DOI hold great promise as tools for cognition and the neurosciences, there are limitations to their application, as well as technological advances that will enhance their application.

Estimation of the oxy- and deoxyhemoglobin concentrations is sensitive to random measurement error and systematic errors arising from incorrect model parameters. Of significant concern is

* Corresponding author. Fax: +1 617 726 7422.

Available online on ScienceDirect (www.sciencedirect.com.)

cross-talk in the estimate of the oxy- and deoxyhemoglobin concentrations. These errors can be partially reduced by judicious choice of measurement wavelengths (Sato et al., 2004; Strangman et al., 2003; Uludag et al., 2002; Yamashita et al., 2001).

The diffuse nature of photon migration through the tissue limits the penetration depth and thus the sensitivity to brain activation occurring subcortically. The sensitivity to brain activation is further compromised by contamination from several systemic physiological signals, which can have a larger percent signal variation than that of the brain activation and in some cases may even phase-lock with the stimulation (Franceschini et al., 2003; Obrig et al., 2000; Toronov et al., 2000).

DOI can potentially achieve spatial resolution of 1 cm in the axes parallel to the scalp in the adult human brain close to the skull (resolution degrades rapidly with increasing depth in the brain). However, current measurement strategies primarily utilize non-overlapping geometric arrangements of sources and detectors, and thus spatial resolution is no better than the typical source-detector separation of 3 cm (Boas et al., 2004). Spatial resolution in the depth axis is significantly worse in adult humans due to the small source-detector separations that can be used (<5 cm). Depth resolution could be improved if transmission measurements were made. However, while this is possible in newborn babies (Hintz et al., 1999), it is generally not possible in adult humans.

The limited depth resolution of DOI causes significant partial volume error and prevents absolute amplitude accuracy in the estimates of the hemoglobin concentration response to brain activation. As a result, quantitative comparison of response amplitudes from different brain regions within a subject and from the same brain region between subjects is compromised. Prior spatial information is required to overcome the partial volume problem. This information can be provided by fMRI if the brain activations measured by fMRI and DOI are correlated in space and time.

Again, NIRS has demonstrated the promise and feasibility of diffuse optical methods as tools for cognition and neuroscience. To realize their full potential, however, diffuse optical imaging methods need further development and implementation. In this paper, we review the current technological issues with diffuse optical imaging and the progress being made towards resolving these issues with example results from our laboratory. Specifically,

1. We review the recent discussion on choosing optimal wavelengths for minimizing noise and cross-talk in the estimate of the hemoglobin concentrations.
2. We discuss the strong presence of systemic physiological signals in the optical data, which interferes with estimates of the hemodynamic response to brain activation, and then present examples of how straightforward signal processing can help to distinguish the different systemic physiological components from the brain activation signal, to ultimately improve the contrast-to-noise ratio estimate of the hemodynamic response function.
3. We review the significant improvement in spatial resolution and relative amplitude accuracy provided by overlapping measurements of the tissue.
4. We emphasize that partial volume error leads to an underestimate of the concentration changes. While this is well known, many papers still report quantitative units for concentrations changes, although only the relative units are accurate. Generally, the relative accuracy is sufficient for brain activation studies.
5. Absolute DOI amplitude accuracy requires better spatial resolution, particularly in depth, as can be provided by spatial prior information from, for example, MRI. We review progress in the spatial-temporal correlation of fMRI and DOI that will provide more insight into the biophysics of their respective signals. Ultimately, the routine combination of fMRI and DOI will provide high spatial-temporal resolution of brain activation with quantitative measures of the hemodynamic, metabolic, and neuronal response to brain activation.

Diffuse optical imaging forward and inverse problem basics

Many researchers (e.g., Furutsu, 1980; Groenhuis et al., 1983; Ishimaru, 1978; Johnson, 1970; Patterson et al., 1989) have shown that the photon fluence rate, $\Phi(\mathbf{r}, t)$ (photons/[cm²·s]), obeys the following diffusion equation in highly scattering media:

$$\nabla \cdot D(\mathbf{r}) \nabla \Phi(\mathbf{r}, t) - v\mu_a(\mathbf{r})\Phi(\mathbf{r}, t) + vS(\mathbf{r}, t) = \frac{\partial \Phi(\mathbf{r}, t)}{\partial t}. \quad (1)$$

$\Phi(\mathbf{r}, t)$ is proportional to the photon number density $U(\mathbf{r}, t)$ (photons/cm³), that is, $\Phi(\mathbf{r}, t) = vU(\mathbf{r}, t)$. The turbid medium is characterized by a speed of light, v , an absorption coefficient μ_a (i.e., the multiplicative inverse of the photon absorption length), and a photon diffusion coefficient, $D = v/3(\mu'_s + \mu_a) \cong v/3(\mu'_s)$; since in most tissues $\mu'_s \gg \mu_a$. The medium's reduced scattering coefficient is defined as $\mu'_s = (1 - g)\mu_s$ and represents the multiplicative inverse of the photon random walk steplength, l^* . Here, μ_s is the reciprocal of the photon scattering length, l , and $g = \langle \cos \theta \rangle$ is the ensemble-averaged cosine of the scattering angle θ associated with a typical single scattering event in the sample; g accounts for the fact that light is more typically scattered in the forward direction, so that many scattering events are required before the initial photon propagation direction is truly randomized. $S(\mathbf{r}, t)$ is an isotropic source term that provides the number of photons emitted at position \mathbf{r} and time t per unit volume per unit time.

The forward solution of the diffusion equation can be obtained for arbitrary tissue geometries with spatially varying optical properties using finite-difference (Barnett et al., 2003; Hielscher et al., 1998), finite-element (Arridge et al., 1993; Okada et al., 1996a; Paulsen and Jiang, 1995), and Monte Carlo (Boas et al., 2002; Graaff et al., 1993; Hayakawa et al., 2001; Hiraoka et al., 1993; Wang et al., 1995) methods. As diffuse optical imaging measurements on the adult human head typically have source-detector separations of 2–4 cm, the head can be considered a semi-infinite medium locally. This simplistic assumption enables an analytic solution of the diffusion equation (Bonner et al., 1987; Haskell et al., 1994; Kienle and Patterson, 1997b) to be used for simulations to test the accuracy and resolution of diffuse optical imaging experiments (Culver et al., 2001; Koizumi et al., 2003). Such simplified simulations are valuable for guiding the optimization of experimental design, which can then be verified with more sophisticated simulations.

The absorption and scattering properties of the tissue are wavelength-dependent. The absorption coefficient of the medium is proportional to the concentration of the different chromophores within the medium. For near-infrared wavelengths of 650 to 950 nm, the dominant chromophores in tissue are oxy- and deoxy-

hemoglobin. Thus, the wavelength-dependent absorption coefficient is given by

$$\mu_a(\lambda) = \varepsilon_{\text{HbO}_2}(\lambda)[\text{HbO}_2] + \varepsilon_{\text{HbR}}(\lambda)[\text{HbR}], \quad (2)$$

where λ indicates the photon wavelength, $\varepsilon_{\text{HbO}_2}(\lambda)$ and $\varepsilon_{\text{HbR}}(\lambda)$ are the intrinsic wavelength-dependent extinction coefficients of oxy- and deoxyhemoglobin, respectively, and $[\text{HbO}_2]$ and $[\text{HbR}]$ are the local hemoglobin concentrations that can vary in space and time. Through spectroscopic measurements of the absorption coefficient, we can thus estimate the hemoglobin concentrations. The possibility exists that near-infrared spectroscopy can also measure the absorption of cytochrome oxidase noninvasively in the human brain. The reader is referred to other publications for that discussion (Uludag et al., 2002; Wobst et al., 2001; Wray et al., 1988).

Generally, the change in detected intensity denoted as a change in optical density, ΔOD , is linearly proportional to a small change in the absorption coefficient

$$\Delta\text{OD}(t, \lambda) = -\log\left(\frac{\Phi(t, \lambda)}{\Phi_0(\lambda)}\right) = \Delta\mu_a(t, \lambda)L(\lambda), \quad (3)$$

where the logarithm is a natural logarithm, Φ_0 is the average detected photon fluence, and L is the effective average pathlength of light through the tissue experiencing the absorption change (Arridge et al., 1992; Delpy et al., 1988). These parameters are wavelength-dependent. The effective pathlength is independent of time when the temporal absorption changes are small. This formulation is known as the modified Beer-Lambert law (Cope and Delpy, 1988; Delpy et al., 1988).

The modified Beer-Lambert law can be generalized for a set of discrete volume elements (i.e., voxels), each having a potentially different absorption change

$$\Delta\text{OD}_i(t, \lambda) = \sum_{j=1}^{N_{\text{vox}}} \Delta\mu_{a,j}(t, \lambda)L_{i,j}(\lambda) \quad (4)$$

where $L_{i,j}$ is the effective pathlength of detected photons for the i th measurement in the j th voxel. Eq. (4) can be written in matrix form as $\mathbf{y} = \mathbf{A}\mathbf{x}$ and can be derived from the photon diffusion equation [Eq. (1)] using the Rylov approximation (Arridge, 1999), which finds

$$L_{i,j} = \Phi_0(\mathbf{r}_{s,i}, \mathbf{r}_j)\Phi_0(\mathbf{r}_j, \mathbf{r}_{d,i}), \quad (5)$$

where $\mathbf{r}_{s,i}$ and $\mathbf{r}_{d,i}$ are the source and detector positions, respectively, for the i th measurement.

This is the basis of image reconstruction algorithms in which an image of $\Delta\mu_a$ (i.e., the vector \mathbf{x}) can be obtained from a set of measurements (i.e., the vector \mathbf{y}) through inversion of the matrix \mathbf{A} (i.e., the effective pathlengths $L_{i,j}$). While several advanced imaging algorithms have been developed—including analytic diffraction tomography approaches (Cheng and Boas, 1998; Li et al., 1997; Matson and Liu, 1999; Schotland, 1997), perturbation approaches (Arridge and Schweiger, 1995; Barbour et al., 1995; O’Leary et al., 1995; Schotland et al., 1993; Yao et al., 1997), the Taylor series expansion approach (Jiang et al., 1996; Paulsen and Jiang, 1995), gradient-based iterative techniques (Arridge and Schweiger, 1998), elliptic systems method (ESM) (Gryzain et al.,

1999; Klivanov et al., 1997), and Bayesian conditioning (Barnett et al., 2003; Eppstein et al., 1999)—the most widely used methods for diffuse optical functional brain imaging incorporate a semi-infinite forward model (Kienle and Patterson, 1997a; Patterson et al., 1989) and either backprojection (Colak et al., 1997; Franceschini et al., 2000; Maki et al., 1995; Walker et al., 1997) or perturbation approaches (Arridge, 1999).

For the usual case of fewer measurements than unknowns, the linear problem is underdetermined and is given by the regularized Moore-Penrose generalized inverse

$$\hat{\mathbf{x}} = \mathbf{A}^T (\mathbf{A}\mathbf{A}^T + \alpha s_{\text{max}} \mathbf{I})^{-1} \mathbf{y}, \quad (6)$$

where \mathbf{I} is the identity matrix, s_{max} is the maximum eigenvalue of $\mathbf{A}\mathbf{A}^T$, and α is the regularization parameter that we set to 10^{-3} in the examples below unless otherwise noted. For comparison, the interpolation backprojection scheme often used to date for functional optical brain imaging is given by (Walker et al., 1997)

$$\hat{\mathbf{x}} = (\mathbf{A}\mathbf{S})^T \mathbf{y}, \quad (7)$$

where the diagonal matrix \mathbf{S} acts to column normalize (1 norm) the matrix \mathbf{A} .

Optimum wavelengths and cross-talk in estimating hemoglobin concentrations

Estimating the oxy- and deoxyhemoglobin concentration changes during brain activation requires measurements at two or more wavelengths. Most published optical results of functional brain activation studies are based on two wavelength measurements, and evidence suggests that two wavelengths can provide sufficient accuracy (Sato et al., 2004; Strangman et al., 2003; Yamashita et al., 2001). We consider the question of what are the best two wavelengths for accurately characterizing the concentration changes.

When choosing the optimum wavelengths, the absorption spectra of the main tissue chromophores in the near infrared, oxy- and deoxyhemoglobin and water should be considered (Wray et al., 1988) (figure not shown due to space limitations). Wavelengths should be chosen in the range of 670 to 900 nm, as shorter wavelengths are too strongly absorbed by hemoglobin, and longer wavelengths are strongly absorbed by water. In addition, to maximize sensitivity to hemoglobin oxygenation changes, it is necessary to choose a wavelength above and below the hemoglobin isobestic point at 805 nm, where oxy- and deoxyhemoglobin have the same intrinsic absorption coefficient. It is common to choose 830 nm as one of the wavelengths as the hemoglobin absorption spectra change little from 830 to 900 nm, and the sensitivity of photomultiplier tubes decreases rapidly above 840 nm. Even in systems with silicon-based photodetectors with sensitivity beyond 900 nm, it is common to use 830 nm. The choice of wavelength below 800 nm has been variable-dependent on the instrument available. Recently, however, a consensus has begun to emerge that pairing 690 or 750 nm with 830 nm is optimal in the sense of minimizing random and systematic errors (Sato et al., 2004; Strangman et al., 2003; Yamashita et al., 2001).

The error in the estimated hemoglobin concentrations is determined from a straightforward error propagation from the

error in the absorption coefficient change. We rewrite Eq. (2) as $\boldsymbol{\mu} = \boldsymbol{\varepsilon} \mathbf{c}$ where the i th element of vector $\boldsymbol{\mu}$ contains the absorption coefficient change for the i th wavelength, the vector \mathbf{c} contains the oxy- and deoxyhemoglobin concentration changes, and the matrix $\boldsymbol{\varepsilon}$ contains the extinction coefficients. The concentration changes are then given by

$$\mathbf{c} = (\boldsymbol{\varepsilon}^T \boldsymbol{\varepsilon})^{-1} \boldsymbol{\varepsilon}^T \boldsymbol{\mu} \quad (8)$$

and random error in $\boldsymbol{\mu}$ gives rise to random error in \mathbf{c} as

$$\sigma_{\mathbf{c}}^2 = \left((\boldsymbol{\varepsilon}^T \boldsymbol{\varepsilon})^{-1} \boldsymbol{\varepsilon}^T \boldsymbol{\sigma}_{\boldsymbol{\mu}} \right) \left((\boldsymbol{\varepsilon}^T \boldsymbol{\varepsilon})^{-1} \boldsymbol{\varepsilon}^T \boldsymbol{\sigma}_{\boldsymbol{\mu}} \right)^T, \quad (9)$$

where $\sigma_{\mathbf{c}}$ is the standard deviation in \mathbf{c} and $\boldsymbol{\sigma}_{\boldsymbol{\mu}}$ is the standard deviation in $\boldsymbol{\mu}$. As discussed by Corlu et al. (2003), the standard deviation in \mathbf{c} can be minimized by minimizing the condition number of $\boldsymbol{\varepsilon}$, which is the ratio of the maximum eigenvalue of $\boldsymbol{\varepsilon}$ to the minimum eigenvalue of $\boldsymbol{\varepsilon}$. Considering two wavelengths spanning from 670 to 900 nm, the condition number is minimized when one wavelength is less than 710 nm and the other is above 830 nm. This calculation assumes that the standard deviation in the estimate of the absorption coefficient is constant with wavelength. In fact, the stronger absorption below 710 nm increases the measurement noise in ΔOD and thus $\Delta \mu_a$. This effect on the estimation of oxygen saturation has been considered in Yamashita et al. (2001) and Zourabian et al. (2000). This wavelength-dependent measurement error results in 680–700 and 750–760 nm being roughly equivalent when paired with 830 nm. Interestingly, the condition number is smaller if 870 or 890 nm is used instead of 830, suggesting that better noise performance would be obtained with that wavelength.

Another source of error is a systematic error in the estimate of the pathlength factor $L(\lambda)$ used to convert the experimental measurement of the change in optical density ΔOD to the change in absorption coefficient [Eq. (3)]. This pathlength factor is generally estimated assuming that the absorption change is uniform throughout the volume of tissue sampled by the detected diffuse light (Delpy et al., 1988; Duncan et al., 1995). In fact, the brain activation is occurring in a small localized volume of the tissue. The correct partial pathlength factor for light that traverses through this small localized volume depends on its position relative to the source and detector, its volume, and the optical properties of the tissues between it and the source and detector. These parameters are generally not known, and for this reason, estimates of the correct pathlength factors generally have systematic errors. These systematic errors can create cross-talk in the estimates of the changes in the hemoglobin concentrations such that a change in oxyhemoglobin may appear as a change in deoxyhemoglobin and vice versa. This issue has been discussed in Boas et al. (2001), Matcher et al. (1995), Mayhew et al. (1999), Kohl et al. (2000) and Uludag et al. (2002).

The sensitivity to cross-talk, resulting from a systematic error, is the same as the sensitivity to random error. Therefore, the sensitivity to cross-talk is minimized using the same wavelengths of light that minimize the sensitivity to random error. The magnitude of the cross-talk can be derived in a few lines of algebraic manipulation of Eqs. (2) and (4) (Strangman et al., 2003; Uludag et al., 2002), showing that

$$\Delta[X]_{\text{estim}} = P\Delta[X]_{\text{real}} + C\Delta[O]_{\text{real}} \quad (10)$$

where $[X]$ represents either $[\text{HbO}_2]$ or $[\text{HbR}]$, and correspondingly, $[O]$ represents the *other* species $[\text{HbR}]$ or $[\text{HbO}_2]$, respectively. P indicates the partial pathlength reduction in the estimated species concentration, and C indicates the cross-talk from the other species, as given by

$$\begin{aligned} P &= \left[\frac{-k(\lambda_1)\varepsilon_X(\lambda_1)\varepsilon_0(\lambda_2) + k(\lambda_2)\varepsilon_0(\lambda_1)\varepsilon_X(\lambda_2)}{[\varepsilon_0(\lambda_1)\varepsilon_X(\lambda_2) - \varepsilon_X(\lambda_1)\varepsilon_0(\lambda_2)]} \right] \\ &= Ak(\lambda_1) + Bk(\lambda_2) \\ C &= \frac{-\varepsilon_0(\lambda_1)\varepsilon_0(\lambda_2)}{\varepsilon_0(\lambda_1)\varepsilon_X(\lambda_2) - \varepsilon_X(\lambda_1)\varepsilon_0(\lambda_2)} [k(\lambda_1) - k(\lambda_2)] \\ &= D[k(\lambda_1) - k(\lambda_2)] \end{aligned} \quad (11)$$

where ε_x and ε_o are the corresponding extinction coefficients, and $k(\lambda) = L_{\text{real}}(\lambda)/L_{\text{estim}}(\lambda)$ indicates the error in the pathlength factor at each wavelength. Note that when the error at each wavelength is the same, the cross-talk $C = 0$. The parameters A , B , and D are simply a function of wavelength and are plotted in (Strangman et al., 2003). The magnitude of D indicates the cross-talk potential, which is minimized with the shorter wavelength below 760 nm.

The appearance of cross-talk is shown in Fig. 1. This simple experiment used a single source and two detectors to measure brain activation of the motor-sensory cortex of the left hemisphere during four blocks of 15 s of right-hand finger extension and flexion and 15 s of rest, using the suboptimal wavelength pair of 780 and 830 nm. The source was posterior to M1 and the two detectors anterior, 3 cm from the source and approximately 1.5 cm from each other. In this way, each detector has a different sampling of the localized change in the cortical absorption coefficient arising

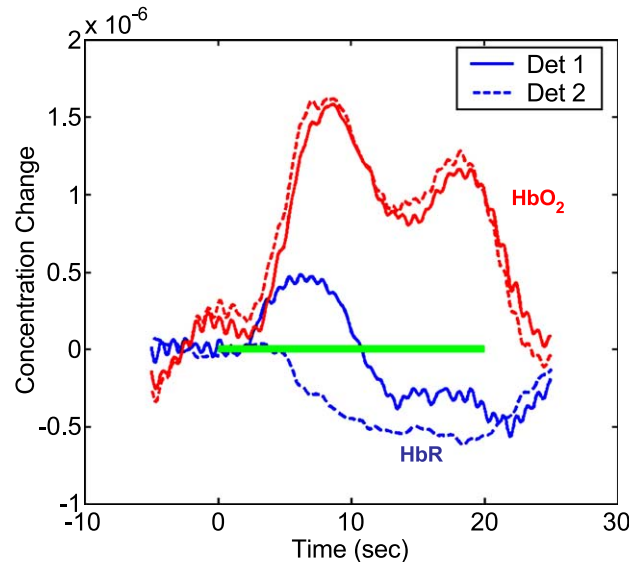


Fig. 1. An example of cross-talk between oxy- (red lines) and deoxyhemoglobin (blue lines) changes during finger-tapping stimulation. Stimulus duration indicated by the horizontal green bar. The cross-talk between oxy- and deoxyhemoglobin for detector 1 is due to the inaccuracy of the pathlength factor. The cross-talk is negligible for detector 2 presumably due to a more accurate estimate of the pathlength factors for the positioning of the detector relative to the brain activation. The same pathlength factors were used for detectors 1 and 2.

from the brain activation, and therefore the correct pathlength factors used for each detector should be different. We followed the typical procedure of using the same pathlength factor of 18 cm for each detector. The estimated hemoglobin concentration changes are shown in Fig. 1. While one detector shows the expected result of a decrease in HbR, the other nearby detector shows an initial increase in HbR followed by a decrease. The HbO₂ response is comparable for both detectors and shows the expected increase with stimulation. Comparison of the HbO₂ and HbR time traces suggests that the biphasic HbR response is cross-talk from HbO₂. The cross-talk of HbR into HbO₂ is not as evident since the HbR concentration change is three times smaller. When we subtract a fraction of the HbO₂ response from the HbR response for the second detector, the HbR response closely resembles the response from the first detector, supporting our suspicion of cross-talk.

The example of cross-talk provided in Fig. 1 indicates that cross-talk does arise in experimental situations. Using the suboptimal wavelength pair of 780 and 830 nm, the potential for cross-talk of HbO₂ into HbR is more than 10 times greater than with a wavelength pair of 690 and 830 nm (as seen from Fig. 3c in Strangman et al., 2003). Choosing the more optimal wavelength pair significantly reduces the sensitivity to cross-talk. Cross-talk is further reduced by ensuring that the measurement is maximally sensitive to the brain activation, that is, by placing the source and detector directly over the region of brain activation (Strangman et al., 2003). Carefully following these guidelines will reduce the contamination of cross-talk, although it will not guarantee that cross-talk will not appear, contrary to that suggested by Sato et al. (2004) and Uludag et al. (2002). Cross-talk always has the potential to appear when model errors are present, as discussed later and shown in Fig. 7f.

Systemic physiological signal interference

In addition to pathlength factor errors giving rise to cross-talk in the estimate of the hemoglobin concentrations, there are numerous sources of systemic signal interference that reduce our sensitivity to weaker brain activation signals. These systemic signals include cardiac pulsations, respiration, and blood pressure variations, including Mayer waves with an approximately 10-s period and other slower variations. In humans, the cardiac pulsation typically has a period of 0.7 to 1.5 s and gives rise to a systemic transient

arterial blood volume increase. Respiration typically has a period of 3 to 8 s and varies thoracic pressure causing a modulation of systemic venous blood volume and a delayed heart rate increase with a corresponding raise in blood pressure. The arterial blood pressure varies on multiple time scales including the cardiac pulsation, respiration, approximately 10-s Mayer waves (Obrig et al., 2000), and slower >50-s variation. Examples of these different systemic signals are seen in Fig. 2, which shows typical traces from the scalp of an adult human compared with independent measures of blood pressure and respiration. These systemic signals also show a strong spatial correlation. This is illustrated in Fig. 2, in which are reported 4 of 50 measurements acquired over the whole head of a subject. The measurements were obtained with source-detector separations of 3 cm using a 32-laser and 32-detector continuous-wave diffuse optical imaging system similar to that described in Franceschini and Boas (2004) and Franceschini et al. (2003). Note that the temporal variation of these systemic signals can be as large as 10%, compared with brain activation signals which are rarely larger than 5% for a strong finger-tapping stimulus and typically much smaller for most other stimuli (Chance et al., 1993; Franceschini et al., 2003; Kennan et al., 2002; Pena et al., 2003). An additional concern is that these systemic signals have been observed to phase-lock with certain types of stimuli, thus confounding the interpretation of the spatial-temporal maps of brain activation.

To improve the optical sensitivity to brain activation, as well as the interpretability of the measured hemodynamic response function, it is necessary to develop signal processing methods that distinguish the different source signals in space and time. While such approaches have been discussed extensively in the fMRI literature where the same systemic signals interfere with the brain activation signal (Lin et al., 2003; Thirion and Faugeras, 2003), there has been little application to diffuse optical imaging. Barbour et al. (2001) have long argued that diffuse optical imaging methods can provide rich physiological information through analysis of the systemic dynamic vascular signals. Prince et al. (2003) have applied state space estimation techniques to the time-varying reconstruction to distinguish cardiac, respiratory, and brain activation signals. Zhang et al. (in press) used a principle component analysis (PCA) to determine the principle spatial components of the spatial-temporal covariance of baseline optical data and then used it to filter systemic signal variation from optical data of brain activation. We will discuss an example of this latter approach in more detail.

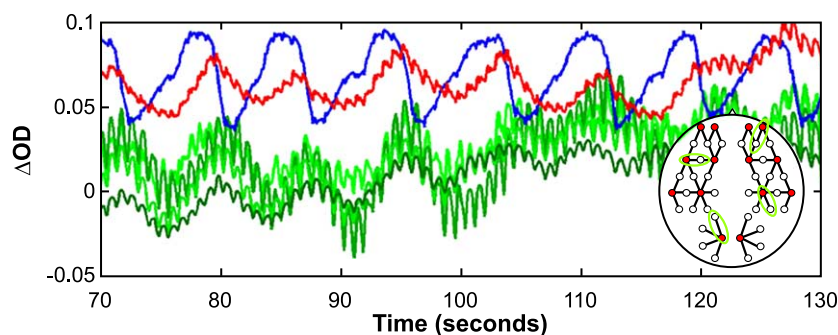


Fig. 2. Optical signal acquired in four positions on the head. The drawing indicates the positions from which the four ΔOD signals were collected. This probe geometry covers most of the adult head. The optical signals in the four head regions are temporally correlated at various time scales and are temporally correlated with the independent measurements of blood pressure (red line) and respiration (blue line). The very slow (30–40 s), slow (approximately 8 s), and fast (1 s) oscillations of the optical signal are strongly correlated with the oscillations of the blood pressure measured with a finger cuff. The approximately 8-s optical oscillations are also correlated with the respiration signal measured with a thoracic strain gauge belt, but delayed by 1–2 s.

A subject performed 10 blocks of 10 s of right hand finger tapping followed by 20 s of rest. Measurements were obtained from 50 different nearest neighbor pairs of sources and detectors as indicated in Figs. 2 and 3a. The data was band-pass-filtered between 0.02 and 0.8 Hz and block-averaged. The block-averaged, spatial-temporal hemodynamic response from 5 s before stimulus onset to 20 s after, for a total duration of 35 s, is shown in Fig. 3a, indicated by the blue curves. The curves reflect the measured increase in optical density at 830 nm. This increase is seen to occur for almost all source-detector pairs over the head. This increase is clearly not localized to contralateral motor cortex. It is, however, strongly correlated with a heart rate increase and associated blood pressure increase observed to be synchronized with the stimulus (data not shown).

We used a principle component analysis of the covariance of 300 s of baseline data (i.e., no stimulus induced brain activation) to identify the major component of spatial covariance in the data as described in Zhang et al. (in press). We then projected out this spatial component of the data after band-pass filtering the stimulus data and before block averaging. The resulting spatial-temporal map of brain activation is shown by the red lines in Fig. 3a, demonstrating an absorption increase that is more localized over the contralateral hemisphere. This is a qualitative observation and suggests that such signal processing can improve the estimate of the hemodynamic response to brain activation. However, further quantitative analysis is required to understand the significance of the benefit particularly in light of the major limiting assumption of orthogonality between the signal components in the principle component analysis (Zhang et al., in press).

The major component of spatial covariance from the baseline data appeared to be effective at filtering the stimulus-induced systemic global response to finger tapping. This suggests that the major component of spatial covariance accounts for the experimentally observed heart rate and systemic blood pressure increase that was synchronized with the stimulus. This hypothesis can be explored by comparing the spatial map of the first component of the PCA with a spatial map of the temporal cross-correlation of the baseline optical data and an independent measure from a real-time

blood pressure finger cuff (homemade device). This comparison is shown in Figs. 3b,c. The similarity is remarkably good and supports the hypothesis.

Furthermore, we compared the second component from the PCA with the cross-correlation of the optical data and an independent measure of respiration (strain gauge belt, Sleepmate/Newlife Technologies, Resp-EZ) and once again found remarkable agreement (Figs. 3d,e). This points to the possibility that, for these types of measurements, a PCA can distinguish the different physiological components of the optical data.

More detailed cross-correlation with independent systemic physiological measures is required to gain greater insight into this source of physiological signal interference to guide development of optimized signal processing algorithms for enhancing sensitivity to brain activation. In addition, quantitative metrics are needed to assess the improvement in the estimated hemodynamic response function. This is a particularly challenging problem as physiologically rigorous models of the hemodynamic response to brain activation require further experimental validation (Buxton and Frank, 1997; Buxton et al., 1998).

Improving image resolution with overlapping measurements

The first diffuse optical images of brain activation were published in 1995 (Maki et al., 1995). For the most part, all such images published to date were produced by analyzing the hemodynamic response measured with individual pairs of sources and detectors and then interpolating the response between the measurement channels, as described in Franceschini et al. (2000) and Maki et al. (1995). The resolution is comparable to the source-detector separation, and quantitative accuracy is compromised because the obtained image is not an optimal solution of the inverse problem (Arridge, 1999). Here, we refer to the image obtained by an optimal solution of the inverse problem as the diffuse optical tomography (DOT) image. There are only a few published examples of DOT images of brain hemodynamics, for example, in rodents (Culver et al., 2003a,b; Siegel et al., 1999), in

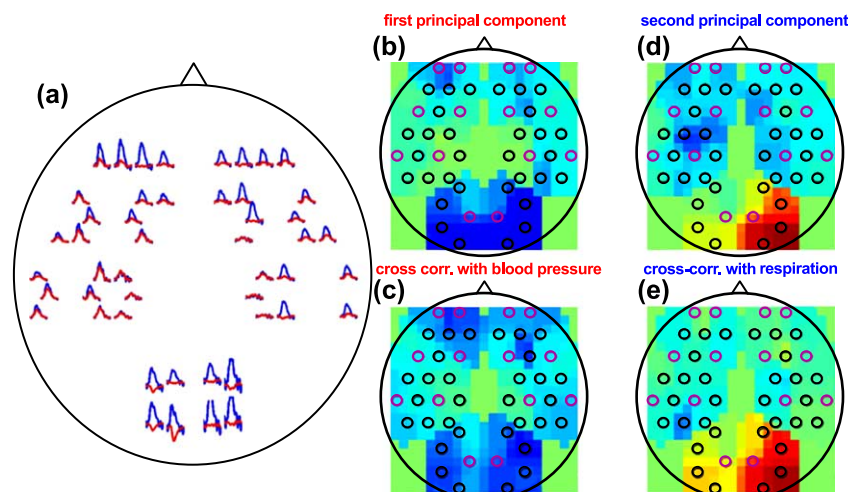


Fig. 3. (a) Spatial-temporal map of brain activation in response to 10 blocks of right hand finger tapping. The blue curves are the ΔOD changes at 830 nm block averaged after a temporal band-pass filter between 0.02 and 0.8 Hz; the red curves are the ΔOD changes obtained after PCA analysis. The x-axis is 35 s long, with the stimulation period lasting for 10 s, followed by 20 s of baseline. The y-axis is from -7% to 7% changes in ΔOD . (b) and (d) Maps of the first and second principal component of the optical data at 830 nm obtained during 300 s of baseline. (c) and (e) Cross-correlation maps of the optical data with the blood pressure (c) and respiration (e) during baseline. The optical data was cross-correlated with blood pressure and respiration with a 2-s lag.

newborn human babies (Hintz et al., 2001), and in adult humans (Bluestone et al., 2001). The advancement of true DOT for brain activation in humans would improve the image spatial resolution and quantitative accuracy over that of current interpolating backprojection methods. This can only be achieved by providing overlapping measurements of the tissue.

We now present simulations that show the dramatic improvement in spatial resolution when overlapping measurements are provided. In a recent paper (Boas et al., 2004), we investigated different probe geometries and concluded that a hexagonal geometry is the best available option because of current technology limitations. We set the longer separation to 4.25 cm, which gave us a shorter separation of 2.5 cm. The absorption imaging matrix \mathbf{A} was calculated using the Rytov approximation for a semi-infinite medium as described above with $\mu'_s = 10 \text{ cm}^{-1}$ and $\mu_a = 0.1 \text{ cm}^{-1}$. The sources and detectors were placed on the planar surface of the medium, and the absorption image was constrained to a plane at a depth of 1.5 to 2.0 cm below the surface. The vector of measurements \mathbf{y} is given by $\mathbf{y} = \mathbf{A} \mathbf{x}$ where the i th element of \mathbf{x} corresponds to the absorption change in the i th voxel in the plane at a depth of 1.5 to 2.0 cm. Given the simulated measurements, the reconstructed image is given by Eq. (6). We compare image resolution obtained with Eq. (6) with that obtained using an interpolation backprojection scheme given by Eq. (7) (Walker et al., 1997). These interpolation images are only shown for nearest neighbor measurements, as this is standard practice in the diffuse optical neuroimaging literature to date.

The image performance depends on the position of the absorption change relative to the sources and detectors. Fig. 4 shows examples of good and bad image performance given a point absorption change in different locations. Basically, when the absorption change occurs in a region that is equally sampled by neighboring measurements, then the images acquired with only nearest neighbor measurements are significantly blurred since the spatial ambiguity of the location of the absorption change cannot be resolved. This extra spatial blurring also results in reduced image amplitude, as shown in Fig. 4a using the interpolation imaging scheme and Fig. 4b using diffuse optical tomography with only nearest neighbor measurements. This ambiguity is resolved by the addition of overlapping measurements from the second nearest neighbor measurements (Fig. 4c). Thus, overlapping measurements provide more spatial uniformity in the image resolution and image amplitude. While not detailed here, overlapping measurements also provide better localization accuracy, as discussed in Boas et al. (2004).

Partial volume errors

As can be seen in Figs. 4a,b, the reconstructed amplitude of the localized absorption change can depend on its position relative to the sources and detectors. This results from what is classically known as a partial volume error. The partial volume error is the imaging equivalent of the partial pathlength factor used in the NIRS community as discussed above. In addition to potentially causing cross-talk, it results in an underestimate of the true concentration error. So, although numerous publications report concentration changes in quantitative units, their results are underestimated due to the partial volume error.

The partial volume error depends on the position of the localized absorption change relative to the positions of the source and detector (especially the depth), the spatial extent of the absorption change, and the optical properties of the tissue. This dependence can be calculated with the photon diffusion equation as illustrated in Strangman et al. (2003). The variation of these parameters limits the ability to compare response amplitude in different brain regions within a subject and the same region between subjects. This partial volume problem is partially addressed by diffuse optical tomographic imaging, which provides more spatial uniformity. This is exemplified in Fig. 4c, which shows comparable amplitudes for the same absorption change in two different locations. Further improvement in quantification requires better depth resolution, as can be provided by time-domain measurements (Kohl-Bareis et al., 2002; Steinbrink et al., 2001) or by prior spatial information from structural and functional MRI. Further discussion of time-domain methods for imaging brain activation falls outside of the scope of this paper.

MRI structural and functional spatial priors for improving quantitative accuracy of diffuse optical imaging

Despite improvements in imaging localization and resolution afforded by overlapping measurements and spectral imaging (Li et al., 2004), the limited depth resolution and spatial extent of the imaging point spread function are likely to render quantitative estimates of the changes in oxy- and deoxyhemoglobin difficult. However, the quantitative accuracy can be improved by providing prior spatial information about the structure of the head and the location of the brain activation, as is provided by structural and functional MRI (Barbour et al., 1995; Barnett et al., 2003; Ntzachristos et al., 2002; Pogue and Paulsen, 1998).

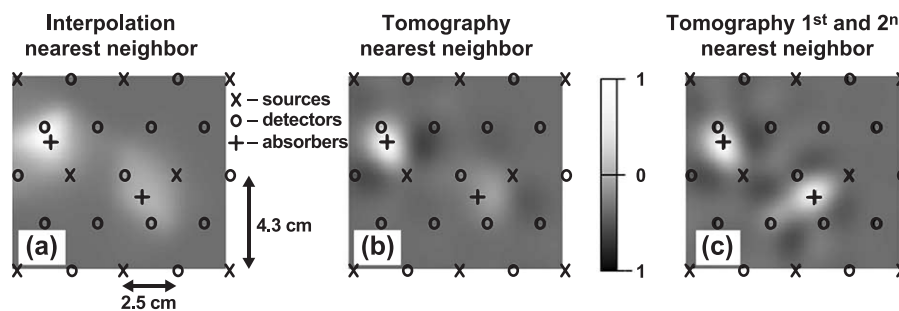


Fig. 4. Comparison of image reconstruction obtained with an interpolation backprojection scheme and with tomography. The sources (x) and detectors (o) positions are superimposed in the images, as well as the positions of the two absorption inhomogeneities (+). Notice that the interpolation image is most blurred and that only the tomography image reveals the two absorbers with equal amplitude. The grey scale goes from -1 to 1 in relative image amplitude units. All methods underestimate the true absorber amplitude due to partial volume effects.

A first step is accurate estimation of the baseline optical properties of the different tissues in the head. In fact, although we are primarily interested in imaging changes in the absorption coefficient, we still need an accurate estimate of the baseline optical properties of the different tissue structures within the head to calculate an accurate imaging matrix for Eq. (6). A procedure for doing this under the guidance of structural MRI has been investigated in Barnett et al. (2003).

Structural and functional MRI can then be used as a spatial prior for DOI of brain activation. The accuracy of this spatial prior depends on the spatial-temporal correlation of fMRI and DOI during brain activation. We first discuss how structural and functional MRI can be used as a spatial prior for DOI and then review the recent advances in exploring their spatial-temporal correlation. We note that the spatial information provided by MRI can either be obtained simultaneously with DOI or collected on a given subject at a separate time. Alternatively, an MRI atlas might be used to guide DOI.

Cortically constrained diffuse optical image reconstruction of brain activation

Given an accurate estimate of the head structure and baseline optical properties, we can then explore the improvement in the quantitative accuracy in the estimate of the localized absorption change caused by brain activation. It is known that the absorption change due to brain activation occurs in the brain and not in the overlying scalp and skull. Thus, given the structure of the head, it is straightforward to constrain the image reconstruction of the brain activation to the cortex. The imaging matrix \mathbf{A} from Eq. (6) can be written as $\mathbf{A} = [\mathbf{A}_{\text{noncortex}} \mathbf{A}_{\text{cortex}}]$ where $\mathbf{A}_{\text{noncortex}}$ has all voxels that are not within the cortex, and $\mathbf{A}_{\text{cortex}}$ contains voxels only from the cortex. The inversion in Eq. (6) produces an image within all of the voxels of the head. We can impose a spatial prior indicating that brain activation and the corresponding absorption change occur only in the cortex by replacing \mathbf{A} in Eq. (6) with $\mathbf{A}_{\text{cortex}}$.

In Fig. 5, we compare the image quality of such a full head reconstruction with a cortically constrained reconstruction. As described above, we used a hexagonal geometry of sources and detectors with first and second nearest neighbor measurements (see Fig 5a). A coronal cross-section of the head is shown in Fig. 5b with the scalp, skull, subarachnoid space, and grey and white matter distinguished. The optical properties for each tissue type were chosen based on the best in vivo estimates available from the literature (Bevilacqua et al., 1999; Okada et al., 1997; Torricelli et al., 2001). For the optical properties, we used $\mu_a = 0.191, 0.136,$

$0.026, 0.186 \text{ cm}^{-1}$ and $\mu'_s = 6.6, 8.6, 0.1, 11.1 \text{ cm}^{-1}$ for scalp, skull, cerebral spinal fluid, and gray and white matter, respectively (Franceschini and Boas, 2004; Strangman et al., 2003). The true simulated brain activation-induced absorption change is depicted in Fig. 5b. The reconstructed absorption change without and with the cortical constraint is shown in Figs. 5c,d, respectively, using a regularization parameter $\alpha = 0.01$ [Eq. (6)]. Note that the absorption change without the cortical constraint is reconstructed in the skull. This is a common problem with minimum norm regularization, which biases the image towards smaller image amplitude and which is accomplished by reconstructing the image in regions with greater measurement sensitivity. For this head geometry, the measurements are significantly more sensitive to the scalp and skull than to the brain, thus pulling the reconstructed absorption change towards the surface of the head and underestimating the magnitude of the absorption change. The cortically constrained image reveals the absorption change in the proper location, but the reconstructed image is flattened towards the cortex near the skull where the measurement sensitivity is greatest. Nonetheless, the reconstructed absorption change with the cortical constraint is within 10% of the true absorption change. This accuracy was achieved because the true absorption change was close to the surface of the head, and its diameter was close to the imaging point-spread function. A smaller diameter absorption change would be reduced by blurring. A true absorption change deeper in the cortex would be reconstructed closer to the surface and thus would have a smaller absorption coefficient.

Depth accuracy, and thus amplitude accuracy, can be further improved by employing a functional MRI of brain activation as a statistical spatial prior for reconstructing the absorption change in a localized region within the cortex. This is similar to work in which an fMRI spatial prior constrains the spatial source localization in the MEG and EEG inverse problem (Dale et al., 2000). A statistical spatial prior has been used in diffuse optical imaging of breast cancer, in which an x-ray mammogram was used as a prior in the diffuse optical image (Li et al., 2003).

Temporal correlation of fMRI and diffuse optical imaging

The appropriateness of fMRI as a statistical spatial prior on the optical image depends on the spatial-temporal correlation of the two different imaging modalities. The fMRI–BOLD signal arises from the paramagnetic properties of deoxyhemoglobin, and thus a correlation is expected between the BOLD signal and the optical deoxyhemoglobin signal. In recent years, a number of studies have been published comparing hemoglobin concentration changes

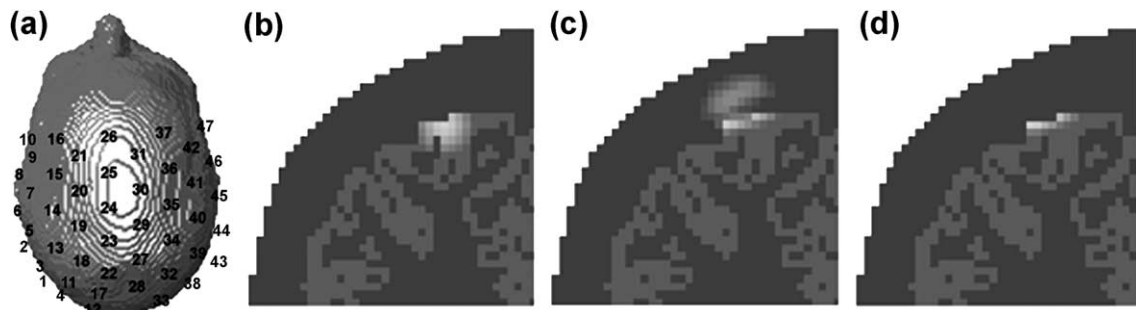


Fig. 5. Comparison of image reconstruction with and without a cortical constraint. (a) Probe geometry on a 3D segmented head. (b) True location of the simulated absorption change. (c) Image reconstructed using DOT and overlapping measurements. (d) Image reconstructed with a cortical constraint.

measured with NIRS and BOLD–fMRI signals in humans (Kleinschmidt et al., 1996; Strangman et al., 2002; Toronov et al., 2001). While all theoretical studies to date support the expectation of a strong correlation between deoxyhemoglobin and BOLD, experimental confirmation remains controversial. In some publications, better temporal correlation between oxyhemoglobin and BOLD has been reported (Hoshi et al., 2001; Strangman et al., 2002), while others (MacIntosh et al., 2003; Siegel et al., 2003; Toronov et al., 2001) have shown better correlation between BOLD and deoxyhemoglobin. This discrepancy in the literature is due to insufficient temporal resolution and low SNR in both the NIRS and fMRI signals.

It is known that a typical hemodynamic response to brain activation is initiated by an increase in blood flow and total hemoglobin (HbT) concentration, possibly preceded by an increase in oxygen consumption (Buxton et al., 1998; Malonek et al., 1997), followed by a venous washout of deoxyhemoglobin delayed by 1 to 2 s relative to the total hemoglobin increase (Frostig et al., 1990; Jaszewski et al., 2003; Kwong et al., 1992; Malonek and Grinvald, 1996; Obrig et al., 1996; Ogawa et al., 1992; Wolf et al., 2002). The initial total hemoglobin increase occurs within the arterial vascular compartment and is concomitant with an increase in oxyhemoglobin. Oxyhemoglobin then increases above total hemoglobin as it displaces deoxyhemoglobin from the veins. Thus, an fMRI and optical comparison with good temporal resolution and signal-to-noise ratio should be able to clearly distinguish a BOLD correlation with deoxyhemoglobin or oxyhemoglobin based on the early temporal response to brain activation. This comparison has been made with an event-related 2-s finger-tapping task by Huppert et al. (2004). Fig. 6a shows the typical hemodynamic response recorded via both modalities for a single subject who performed 27 instances of the task in 6 min. The hemodynamic response begins within 1–3 s following the start of subject finger tapping, with the expected increase in oxyhemoglobin preceding that in deoxyhemoglobin by approximately 1.5 s. A cross-correlation comparison between normalized BOLD and optical response profiles showed significant differences from zero for the period 0- to 15-s poststimulus onset and yielded R values of 0.976, 0.781, and 0.636 for the zero-lag coefficients between HbR/BOLD, HbO₂/BOLD, and HbT/BOLD, respectively [P values = $5.52e-20$; $3.47e-7$; $1.65e-4$]. The BOLD response was also shifted by 1.5 s relative to the onset of the oxyhemoglobin response and aligned

fully with the deoxyhemoglobin profile, as shown in the normalized comparison of the responses in Fig. 6b.

These data clearly indicate that the BOLD signal correlates more strongly with the optical measurements of HbR than with HbO₂ and HbT, in agreement with theoretical expectations. Confirmation of this temporal correlation on additional subjects will further motivate the use of the fMRI–BOLD signal as a spatial prior for DOI to improve the quantitative estimate of the HbR change during activation. But first, a detailed spatial correlation of DOI and fMRI is required.

Spatial correlation of fMRI and diffuse optical imaging

Comparisons of the spatial correlation of fMRI and DOI are beginning to appear in the literature (Kleinschmidt et al., 1996; Strangman et al., 2002; Toronov et al., 2001). The spatial correlation is strong in the somatosensory cortex of the rat (Culver et al., 2003b). This comparison is aided by the good optical resolution afforded by overlapping measurements. In our experience with human subjects, while a qualitative spatial correlation is easy to observe, it has been difficult to find a strong quantitative spatial correlation. In our experience with simultaneous fMRI and DOI, we often observe the DOI localized activation displaced 2 to 3 cm from the fMRI when we expect to find them spatially coregistered. This discrepancy could easily result from the spatial transformation between the MRI coordinate system and the DOI coordinate system. While the MRI coordinate system is in true 3D space, DOI images are usually produced assuming a flat planar surface underneath the array of sources and detectors. This distortion from the curved surface of the head to a flat surface could produce the spatial misregistration of fMRI and DOI that is often observed.

To overcome this problem, the optical images need to be reconstructed within the proper curved surface of the head and with the cortical constraint, since we know from simulation studies that otherwise the DOI depth will be incorrect, possibly producing a bias in the lateral coordinates. Alternatively, as a first step, the fMRI brain activation image can be radially projected within coronal slices onto the surface of the scalp for comparison with the measured optical signals. The channel with the maximum optical response to brain activation should correspond to the source-detector pair that is closest to the

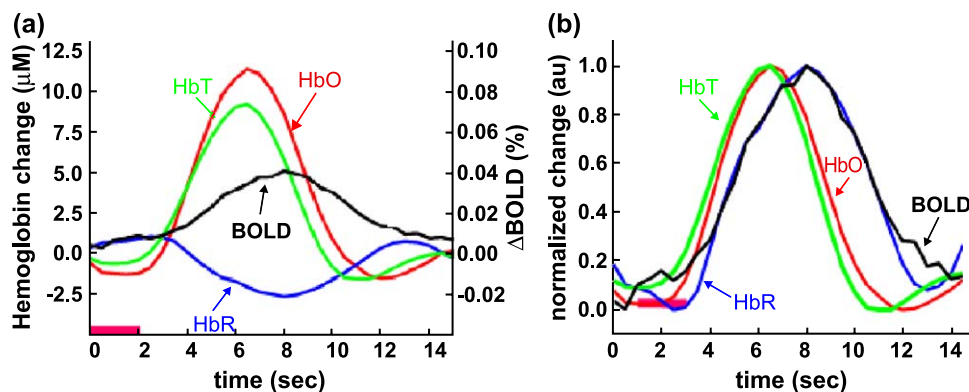


Fig. 6. (a) Response functions of hemoglobin concentrations and BOLD for event-related finger tapping as measured through simultaneously acquired fMRI–BOLD and DOI optical recordings of the primary motor cortex. (b) Normalized and rescaled response functions for the event-related finger tapping to allow visualization of the four variables on the same linear scale. The deoxyhemoglobin data have also been inverted to emphasize the strong correlation between deoxyhemoglobin and BOLD.

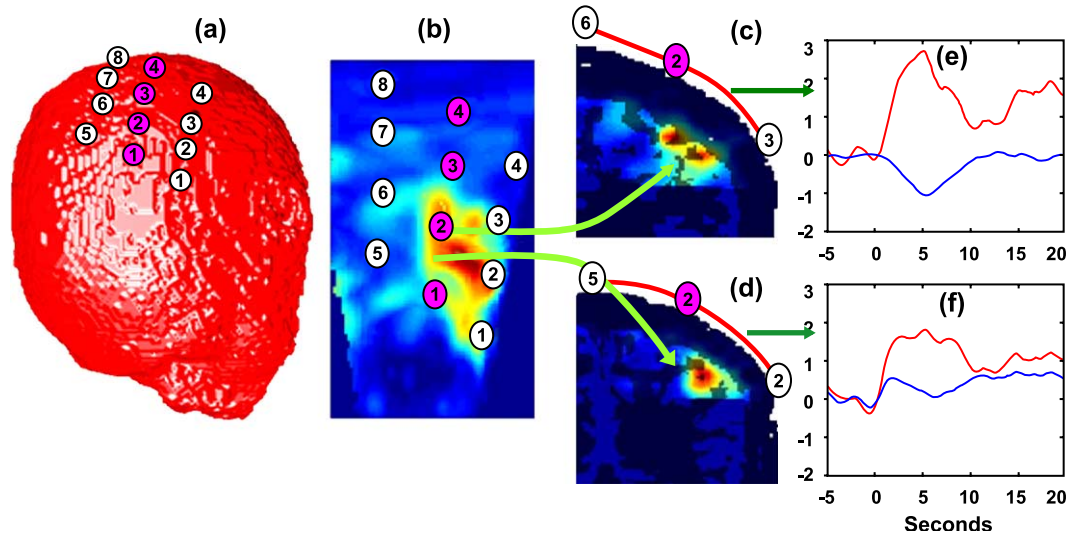


Fig. 7. (a) Coregistration of the position of optical sources (pink) and detectors (white) on the structural MRI of the subject. (b) Maximum intensity radial projection of the fMRI t statistic image on to the scalp. The source and detector positions are overlaid to reveal the spatial correlation of the optical signals and the BOLD signal. (c) and (d) Coronal slices through the maximum fMRI response (d) and 1 cm posterior (c). (e) and (f) Hemoglobin concentration time traces measured with source 2 and detectors 3 and 2, respectively, in relative units. Red oxyhemoglobin, blue deoxyhemoglobin. The stimulus starts at $t = 0$ s and lasts 2 s.

maximum fMRI response as projected onto the surface of the scalp.

We have begun to perform this latter comparison and show our first result in Fig. 7. A structural MRI of the subject was obtained to provide anatomical guidance for the fMRI and to localize the fiber optic fiducials on the scalp. The array of four sources and eight detectors localized on the scalp is shown in Fig. 7a. The sources delivered light to the scalp at 690 and 830 nm. The nearest neighbor distance between sources and detectors was 3.0 cm, while the distance between sources and between detectors was 1.9 cm. The same event-related finger-tapping paradigm as shown above for the temporal correlation was used for the spatial correlation. A maximum intensity radial projection of the fMRI t statistic image on to the scalp performed in each coronal slice is shown in Fig. 7b with the overlay of the optical sources and detectors. From this flattened projection, it is clear that the most significant fMRI response occurs between source 2 and detector 2. In Figs. 7e,f, we show the optical estimates of the hemoglobin concentration changes measured with source 2 and detectors 3 and 2, respectively. Our most significant optical response was found posterior to the fMRI response between source 2 and detector 3. An inspection of the coronal slices through the maximum fMRI response and 1 cm posterior in the region of the maximum optical response (Figs. 7d,c, respectively) reveals a slightly less significant fMRI response in the region of the maximum optical response. Significantly, however, this more posterior fMRI response is more superficial in the cortex and closer to the surface of the head, such that the optical measurement has higher sensitivity. Interestingly, the more anterior response is deeper in the brain, and the corresponding optical measurement between source 2 and detector 2 appears to have some cross-talk of HbO₂ into HbR, as could result from improper modeling of the pathlength factors due to the depth of the brain activation.

It is clear that this type of spatial comparison can provide quantitative details about the spatial correlation of BOLD and DOI. This first example underscores the importance of consid-

ering the depth of the fMRI response when exploring the spatial correlation with DOI, as the DOI sensitivity drops exponentially with depth.

Summary

Near-infrared spectroscopy is able to measure hemodynamic, metabolic (Boas et al., 2003; Heekeren et al., 1999), and fast neuronal responses to brain activation (Franceschini and Boas, 2004; Gratton et al., 1997; Steinbrink et al., 2000; Wolf et al., 2002) with inexpensive and portable instrumentation. These capabilities are making NIRS, in its present technological state, an important tool in cognition and the neurosciences. The extension of NIRS to diffuse optical imaging will improve the sensitivity, resolution, and accuracy of the optical estimates of the hemodynamic response to brain activation (as well as the metabolic and neuronal response). We identified many issues and illustrated some potential solutions that should be further addressed and explored with much research over the next several years.

Acknowledgments

We thank all of the past and present members of the Photon Migration Laboratory and Martinos Center who have contributed significantly to the development and application of NIRS and DOI. They are too numerous to list here, but their efforts are cited in the paper. We gratefully acknowledge the as yet unpublished contributions of Ted Huppert, Rick Hoge, Jane Andre, and Bruce Fischl, and the critical comments provided by Sol Diamond, Heather Bortfeld, and Gary Boas on drafts of this paper. This work was supported by NIH P41-RR14075, R01-EB002482, R01-EB00790, and CIMIT through the U.S. Army, under Cooperative Agreement No. DAMD17-99-2-9001. This publication does not necessarily reflect the position or the policy of the Government, and no official endorsement should be inferred.

References

- Adelson, P.D., Nemoto, E., Scheuer, M., Painter, M., Morgan, J., Yonas, H., 1999. Noninvasive continuous monitoring of cerebral oxygenation pericrally using near-infrared spectroscopy: a preliminary report. *Epilepsia* 40, 1484–1489.
- Arridge, S.R., 1999. Optical tomography in medical imaging. *Inverse Problems* 15, R41–R93.
- Arridge, S.R., Schweiger, M., 1995. Photon-measurement density functions. Part2: Finite-element-method calculations. *Appl. Opt.* 34, 8026–8037.
- Arridge, S.R., Schweiger, M., 1998. A gradient-based optimisation scheme for optical tomography. *Opt. Express* 2, 213–226.
- Arridge, S.R., Cope, M., Delpy, D.T., 1992. The theoretical basis for the determination of optical pathlengths in tissue: temporal and frequency analysis. *Phys. Med. Biol.* 37, 1531–1560.
- Arridge, S.R., Schweiger, M., Hiraoka, M., Delpy, D.T., 1993. A finite element approach for modeling photon transport in tissue. *Med. Phys.* 20, 299–309.
- Barbour, R.L., Graber, H.L., Chang, J., Barbour, S.S., Koo, P.C., Aronson, R., 1995. MRI-guided optical tomography: prospects and computation for a new imaging method. *IEEE Comput. Sci. Eng.* 2, 63–77.
- Barbour, R.L., Graber, H.L., Pei, Y., Zhong, S., Schmitz, C.H., 2001. Optical tomographic imaging of dynamic features of dense-scattering media. *J. Opt. Soc. Am. A, Opt. Image Sci. Vis.* 18, 3018–3036.
- Barnett, A.H., Culver, J.P., Sorensen, A.G., Dale, A., Boas, D.A., 2003. Robust inference of baseline optical properties of the human head with three-dimensional segmentation from magnetic resonance imaging. *Appl. Opt.* 42, 3095–3108.
- Bevilacqua, F., Pignatelli, D., Marquet, P., Gross, J.D., Tromberg, B.J., Depierreux, C., 1999. In vivo local determination of tissue optical properties: applications to human brain. *Appl. Opt.* 38, 4939–4950.
- Bluestone, A., Abdoulaev, G., Schmitz, C., Barbour, R., Hielscher, A., 2001. Three-dimensional optical tomography of hemodynamics in the human head. *Opt. Express* 9, 272–286.
- Boas, D.A., Gaudette, T., Strangman, G., Cheng, X., Marota, J.J.A., Mandeville, J.B., 2001. The accuracy of near infrared spectroscopy and imaging during focal changes in cerebral hemodynamics. *NeuroImage* 13, 76–90.
- Boas, D.A., Culver, J., Stott, J., Dunn, A.K., 2002. Three dimensional Monte Carlo code for photon migration through complex heterogeneous media including the adult head. *Opt. Express* 10, 159–170.
- Boas, D.A., Strangman, G., Culver, J.P., Hoge, R.D., Jaszczewski, G., Poldrack, R.A., Rosen, B.R., Mandeville, J.B., 2003. Can the cerebral metabolic rate of oxygen be estimated with near-infrared spectroscopy? *Phys. Med. Biol.* 48, 2405–2418.
- Boas, D.A., Chen, K., Grebert, D., Franceschini, M.A., 2004. Improving diffuse optical imaging spatial resolution of cerebral hemodynamic response to brain activation in humans. *Opt. Lett.* 29, 1506–1508.
- Bonner, R.F., Nossal, R., Havlin, S., Weiss, G.H., 1987. Model for photon migration in turbid biological media. *J. Opt. Soc. Am. A* 4, 423–432.
- Buxton, R.B., Frank, L.R., 1997. A model for the coupling between cerebral blood flow and oxygen metabolism during neural stimulation. *J. Cereb. Blood Flow Metab.* 17, 64–72.
- Buxton, R.B., Wong, E.C., Frank, L.R., 1998. Dynamics of blood flow and oxygenation changes during brain activation: the balloon model. *Magn. Reson. Med.* 39, 855–864.
- Chance, B., Zhuang, Z., UnAh, C., Alter, C., Lipton, L., 1993. Cognitive activated low frequency modulation of light absorption in human brain. *Proc. Natl. Acad. Sci. U. S. A.* 90, 2660–2774.
- Chen, W.G., Li, P.C., Luo, Q.M., Zeng, S.Q., Hu, B., 2000. Hemodynamic assessment of ischemic stroke with near-infrared spectroscopy. *Space Med. Med. Eng. (Beijing)* 13, 84–89.
- Cheng, X., Boas, D.A., 1998. Diffuse optical reflectance tomography with continuous-wave illumination. *Opt. Express* 3, 118–123.
- Colak, S.B., Papaioannou, D.G., Hooft, G.W., van der Mark, M.B., Schomberg, H., Paasschens, J.C.J., Melissen, J.B.M., Van Asten, N.A.A.J., 1997. Tomographic image reconstruction from optical projections in light-diffusing media. *Appl. Opt.* 36, 180–213.
- Colier, W.N., Quaresima, V., Oeseburg, B., Ferrari, M., 1999. Human motor-cortex oxygenation changes induced by cyclic coupled movements of hand and foot. *Exp. Brain Res.* 129, 457–461.
- Cope, M., Delpy, D.T., 1988. System for long-term measurement of cerebral blood flow and tissue oxygenation on newborn infants by infrared transillumination. *Med. Biol. Eng. Comput.* 26, 289–294.
- Corlu, A., Durduran, T., Choe, R., Schweiger, M., Hillman, E.M., Arridge, S.R., Yodh, A.G., 2003. Uniqueness and wavelength optimization in continuous-wave multispectral diffuse optical tomography. *Opt. Lett.* 28, 2339–2341.
- Culver, J.P., Ntzichristos, V., Holboke, M.J., Yodh, A.G., 2001. Optimization of optode arrangements for diffuse optical tomography: a singular-value analysis. *Opt. Lett.* 26, 701–703.
- Culver, J.P., Durduran, T., Furuya, D., Cheung, C., Greenberg, J.H., Yodh, A.G., 2003. Diffuse optical tomography of cerebral blood flow, oxygenation, and metabolism in rat during focal ischemia. *J. Cereb. Blood Flow Metab.* 23, 911–924.
- Culver, J.P., Siegel, A.M., Boas, D.A., 2003. Three dimensional diffuse optical tomography of fore-paw stimulation in a rodent. *Opt. Lett.* 28, 2061–2063.
- Dale, A.M., Liu, A.K., Fischl, B.R., Buckner, R.L., Belliveau, J.W., Lewine, J.D., Halgren, E., 2000. Dynamic statistical parametric mapping: combining fMRI and MEG for high-resolution imaging of cortical activity. *Neuron* 26, 55–67.
- Davis, T.L., Kwong, K.K., Weisskoff, R.M., Rosen, B.R., 1998. Calibrated functional MRI: mapping the dynamics of oxidative metabolism. *Proc. Natl. Acad. Sci. U. S. A.* 95, 1834–1839.
- Delpy, D.T., Cope, M., van der Zee, P., et al., 1988. Estimation of optical pathlength through tissue from direct time of flight measurement. *Phys. Med. Biol.* 33, 1433–1442.
- Duncan, A., Meek, J.H., Clemence, M., Elwell, C.E., Tyszczyk, L., Cope, M., Delpy, D.T., 1995. Optical pathlength measurements on adult head, calf and forearm and the head of the newborn infant using phase resolved optical spectroscopy. *Phys. Med. Biol.* 40, 295–304.
- Eppstein, M.J., Dougherty, D.E., Troy, T.L., Sevick-Muraca, E.M., 1999. Biomedical optical tomography using dynamic parameterization and Bayesian conditioning on photon migration measurements. *Appl. Opt.* 38, 2138–2150.
- Eschweiler, G.W., Wegerer, C., Schlotter, W., Spandl, C., Stevens, A., Bartels, M., Buchkremer, G., 2000. Left prefrontal activation predicts therapeutic effects of repetitive transcranial magnetic stimulation (rTMS) in major depression. *Psychiatry Res.* 99, 161–172.
- Fallgatter, A.J., Strik, W.K., 2000. Reduced frontal functional asymmetry in schizophrenia during a cued continuous performance test assessed with near-infrared spectroscopy. *Shizophr. Bull.* 26, 913–919.
- Fallgatter, A.J., Roesler, M., Sitzmann, L., Heidrich, A., Mueller, T.J., Strik, W.K., 1997. Loss of functional hemispheric asymmetry in Alzheimer's dementia assessed with near-infrared spectroscopy. *Brain Res. Cogn. Brain Res.* 6, 67–72.
- Franceschini, M.A., Boas, D.A., 2004. Noninvasive measurement of neuronal activity with near-infrared optical imaging. *NeuroImage* 21, 336–372.
- Franceschini, M.A., Toronov, V., Filiaci, M., Gratton, E., Fantini, S., 2000. On-line optical imaging of the human brain with 160-ms temporal resolution. *Opt. Express* 6, 49–57.
- Franceschini, M.A., Fantini, S., Thompson, J.H., Culver, J.P., Boas, D.A., 2003. Hemodynamic evoked response of the sensorimotor cortex measured non-invasively with near infrared optical imaging. *Psychophysiology* 40, 548–560.
- Frostig, R.D., Lieke, E.E., Grinvald, A., 1990. Cortical functional architecture and local coupling between neuronal activity and the microcirculation revealed by in vivo high-resolution optical imaging of intrinsic signals. *Proc. Natl. Acad. Sci. U. S. A.* 87, 6082–6086.

- Furutsu, K., 1980. On the diffusion equation derived from the space–time transport equation. *J. Opt. Soc. Am. A* 70, 360.
- Graaff, R., Koelink, M.H., de Mul, F.F., Zijlstra, M., Dassel, W.G., Aarnoudse, M., 1993. Condensed Monte Carlo simulations for the description of light transport. *Appl. Opt.* 32, 426–434.
- Gratton, G., Fabiani, M., Corballis, P.M., Hood, D.C., Goodman-Wood, M.R., Hirsch, J., Kim, K., Friedman, D., Gratton, E., 1997. Fast and localized event-related optical signals (EROS) in the human occipital cortex: comparisons with the visual evoked potential and fMRI. *NeuroImage* 6, 168–180.
- Groenhuis, R.A., Ferwerda, J., Ten Bosch, H.A., 1983. Scattering and absorption of turbid materials determined from reflection measurements: I. Theory. *Appl. Opt.* 22, 2456.
- Gryazin, Y.A., Klivanov, M.V., Lucas, T.R., 1999. Imaging the diffusion coefficient in a parabolic inverse problem in optical tomography. *Inverse Problems* 1, 373–397.
- Hanlon, E.B., Itzkan, I., Dasari, R.R., Feld, M.S., Ferrante, R.J., McKee, A.C., Lathi, D., Kowall, N.W., 1999. Near-infrared fluorescence spectroscopy detects Alzheimer's disease in vitro. *Photochem. Photobiol.* 70, 236–242.
- Haskell, R.C., Svaasand, L.O., Tsay, T., Feng, T., McAdams, M.S., Tromberg, B.J., 1994. Boundary conditions for the diffusion equation in radiative transfer. *J. Opt. Soc. Am. A* 11, 2727–2741.
- Hayakawa, C.K., Spanier, J., Bevilacqua, F., Dunn, A.K., You, J.S., Tromberg, B.J., Venugopalan, V., 2001. Perturbation Monte Carlo methods to solve inverse photon migration problems in heterogeneous tissues. *Opt. Lett.* 26, 1335–1337.
- Heekeren, H.R., Obrig, H., Wenzel, R., Eberle, K., Ruben, J., Villringer, K., Kurth, R., Villringer, A., 1997. Cerebral haemoglobin oxygenation during sustained visual stimulation—A near-infrared spectroscopy study. *Philos. Trans. R. Soc. Lond., B Biol. Sci.* 352, 743–750.
- Heekeren, H.R., Kohl, M., Obrig, H., Wenzel, R., von Pannwitz, W., Macher, S.J., Dirnagl, U., Cooper, C.E., Villringer, A., 1999. Non-invasive assessment of changes in cytochrome-*c* oxidase oxidation in human subjects during visual stimulation. *J. Cereb. Blood Flow Metab.* 19, 592–603.
- Hielscher, A.H., Alcouffe, R.E., Barbour, R.L., 1998. Comparison of finite-difference transport and diffusion calculations for photon migration in homogeneous and heterogeneous tissues. *Phys. Med. Biol.* 43, 1285–1302.
- Hintz, S.R., Cheong, W.F., van Houten, J.P., Stevenson, D.K., Benaron, D.A., 1999. Bedside imaging of intracranial hemorrhage in the neonate using light: comparison with ultrasound, computed tomography, and magnetic resonance imaging. *Pediatr. Res.* 45, 54–59.
- Hintz, S.R., Benaron, D.A., Siegel, A.M., Zourabian, A., Stevenson, D.K., Boas, D.A., 2001. Bedside functional imaging of the premature infant brain during passive motor activation. *J. Perinat. Med.* 29, 335–343.
- Hiraoka, M., Firbank, M., Essenpreis, M., Cope, M., Arridge, S.R., van der Zee, P., Delpy, D.T., 1993. A Monte Carlo investigation of optical pathlength in inhomogeneous tissue and its application to near-infrared spectroscopy. *Phys. Med. Biol.* 38, 1859–1876.
- Hirth, C., Obrig, H., Villringer, K., Thiel, A., Bernarding, J., Muhlnickel, W., Flor, H., Dirnagl, U., Villringer, A., 1996. Non-invasive functional mapping of the human motor cortex using near-infrared spectroscopy. *NeuroReport* 7, 1977–1981.
- Hock, C., Villringer, K., Muller-Spahn, F., Hofmann, M., Schuh-Hofer, S., Heekeren, H., Wenzel, R., Dirnagl, U., Villringer, A., 1996. Near infrared spectroscopy in the diagnosis of Alzheimer's disease. *Ann. N. Y. Acad. Sci.* 777, 22–29.
- Hoge, R.D., Atkinson, J., Gill, B., Crelier, G.R., Marrett, S., Pike, G.B., 1999. Linear coupling between cerebral blood flow and oxygen consumption in activated human cortex. *Proc. Natl. Acad. Sci. U. S. A.* 96, 9403–9408.
- Hoshi, Y., Kobayashi, N., Tamura, M., 2001. Interpretation of near-infrared spectroscopy signals: a study with a newly developed perfused rat brain model. *J. Appl. Physiol.* 90, 1657–1662.
- Huppert, T.J., Hoge, R.D., Franceschini, M.A., Boas, D.A., 2004. A temporal comparison of simultaneously acquired BOLD fMRI and near infrared spectroscopy (NIRS) hemodynamic response functions. *NeuroImage, Suppl.* 1, 24.
- Ishimaru, A., 1978. *Wave propagation and scattering in random media.* (San Diego: Academic Press Inc.).
- Jaszewski, G., Strangman, G., Wagner, J., Kwong, K.K., Poldrack, R.A., Boas, D.A., 2003. Differences in the hemodynamic response to event-related motor and visual paradigms as measured by near-infrared spectroscopy. *NeuroImage* 20, 479–488.
- Jiang, H., Paulsen, K.D., Osterberg, U.L., Pogue, B.W., Patterson, M.S., 1996. Optical image reconstruction using frequency-domain data: simulations and experiments. *J. Opt. Soc. Am. A* 13, 253–266.
- Johnson, C.C., 1970. Optical diffusion in blood. *IEEE Trans. Biomed. Eng. BME17*, 129–133.
- Kennan, R.P., Horowitz, S.G., Maki, A., Yamashita, Y., Koizumi, H., Gore, J.C., 2002. Simultaneous recording of event-related auditory oddball response using transcranial near infrared optical topography and surface EEG. *NeuroImage* 16, 587–592.
- Kienle, A., Patterson, M.S., 1997a. Determination of the optical properties of semi-infinite turbid media from frequency-domain reflectance close to the source. *Phys. Med. Phys.* 42, 1801–1819.
- Kienle, A., Patterson, M.S., 1997b. Improved solutions of the steady-state and the time-resolved diffusion equations for reflectance from semi-infinite turbid medium. *J. Opt. Soc. Am.* 14, 246–254.
- Kleinschmidt, A., Obrig, H., Requardt, M., Merboldt, K.D., Dirnagl, U., Villringer, A., Frahm, J., 1996. Simultaneous recording of cerebral blood oxygenation changes during human brain activation by magnetic resonance imaging and near-infrared spectroscopy. *J. Cereb. Blood Flow Metab.* 16, 817–826.
- Klivanov, M.V., Lucas, T.R., Frank, R.M., 1997. A fast and accurate imaging algorithm in optical/diffusion tomography. *Inverse Problems* 13, 1341–1361.
- Kohl, M., Lindauer, U., Royl, G., Kuhl, M., Gold, L., Villringer, A., Dirnagl, U., 2000. Physical model for the spectroscopic analysis of cortical intrinsic optical signals. *Phys. Med. Biol.* 45, 3749–3764.
- Kohl-Bareis, M., Obrig, H., Steinbrink, J., Malak, J., Uludag, K., Villringer, A., 2002. Noninvasive monitoring of cerebral blood flow by a dye bolus method: separation of brain from skin and skull signals. *J. Biomed. Opt.* 7, 464–470.
- Koizumi, H., Yamamoto, T., Maki, A., Yamashita, Y., Sato, H., Kawaguchi, H., Ichikawa, N., 2003. Optical topography: practical problems and new applications. *Appl. Opt.* 42, 3054–3062.
- Kwong, K.K., Belliveau, J.W., Chesler, D.A., Goldberg, I.E., Weisskoff, R.M., Poncelet, B.P., Kennedy, D.N., Hoppel, B.E., Cohen, M.S., Turner, R., Cheng, H.-M., Brady, T.J., Rosen, B.R., 1992. Dynamic magnetic resonance imaging of human brain activity during primary sensory stimulation. *Proc. Natl. Acad. Sci. U. S. A.* 89, 5675–5679.
- Li, X.D., Durduran, T., Yodh, A.G., Chance, B., Pattanayak, D.N., 1997. Diffraction tomography for biomedical imaging with diffuse photon density waves: errata. *Opt. Lett.* 22, 1198.
- Li, A., Miller, E.L., Kilmer, M.E., Brukilacchio, T.J., Chaves, T., Stott, J., Zhang, Q., Wu, T., Chorlton, M., Moore, R.H., Kopans, D.B., Boas, D.A., 2003. Tomographic optical breast imaging guided by three-dimensional mammography. *Appl. Opt.* 42, 5181–5190.
- Li, A., Zhang, Q., Culver, J.P., Miller, E.L., Boas, D.A., 2004. Reconstructing chromosphere concentration images directly by continuous-wave diffuse optical tomography. *Opt. Lett.* 29, 256–258.
- Lin, F.H., McIntosh, A.R., Agnew, J.A., Eden, G.F., Zeffiro, T.A., Belliveau, J.W., 2003. Multivariate analysis of neuronal interactions in the generalized partial least squares framework: simulations and empirical studies. *NeuroImage* 20, 625–642.
- MacIntosh, B.J., Klassen, L.M., Menon, R.S., 2003. Transient hemodynamics during a breath hold challenge in a two part functional imaging study with simultaneous near-infrared spectroscopy in adult humans. *NeuroImage* 20, 1246–1252.

- Maki, A., Yamashita, Y., Ito, Y., Watanabe, E., Mayanagi, Y., Koizumi, H., 1995. Spatial and temporal analysis of human motor activity using noninvasive NIR topography. *Med. Phys.* 22, 1997–2005.
- Malonek, D., Grinvald, A., 1996. Interactions between electrical activity and cortical microcirculation revealed by imaging spectroscopy: implications for functional brain mapping. *Science* 272, 551–554.
- Malonek, D., Dirnagl, U., Lindauer, U., Yamada, K., Kanno, I., Grinvald, A., 1997. Vascular imprints of neuronal activity: relationships between the dynamics of cortical blood flow, oxygenation, and volume changes following sensory stimulation. *Proc. Natl. Acad. Sci. U. S. A.* 94, 14826–14831.
- Matcher, S.J., Elwell, C.E., Cooper, C.E., Cope, M., Delpy, D.T., 1995. Performance comparison of several published tissue near-infrared spectroscopy algorithms. *Anal. Biochem.* 227, 54–68.
- Matson, C.L., Liu, H.L., 1999. Analysis of the forward problem with diffuse photon density waves in turbid media by use of a diffraction tomography model. *JOSA A* 16, 455–466.
- Matsuo, K., Kato, T., Fukuda, M., Kato, N., 2000. Alteration of hemoglobin oxygenation in the frontal region in elderly depressed patients as measured by near-infrared spectroscopy. *J. Neuropsychiatry Clin. Neurosci.* 12, 465–471.
- Mayhew, J., Zheng, Y., Hou, Y., Vuksanovic, B., Berwick, J., Askew, S., Coffey, P., 1999. Spectroscopic analysis of changes in remitted illumination: the response to increased neural activity in brain. *NeuroImage* 10, 304–326.
- Meek, J.H., Elwell, C.E., Khan, M.J., Romaya, J., Wyatt, J.S., Delpy, D.T., Zeki, S., 1995. Regional changes in cerebral haemodynamics as a result of a visual stimulus measured by near infrared spectroscopy. *Proc. R. Soc. Lond., B* 261, 351–356.
- Nemoto, E.M., Yonas, H., Kassam, A., 2000. Clinical experience with cerebral oximetry in stroke and cardiac arrest. *Crit. Care Med.* 28, 1052–1054.
- Ntziachristos, V., Yodh, A.G., Schnall, M., Chance, B., 2002. MRI-guided diffuse optical spectroscopy of malignant and benign breast lesions. *Neoplasia* 4, 347–354.
- Obrig, H., Hirth, C., Junge-Hulsing, J.G., Doge, C., Wolf, T., Dirnagl, U., Villringer, A., 1996. Cerebral oxygenation changes in response to motor stimulation. *J. Appl. Physiol.* 81, 1174–1183.
- Obrig, H., Neufang, M., Wenzel, R., Kohl, M., Steinbrink, J., Einhaupl, K., Villringer, A., 2000. Spontaneous low frequency oscillations of cerebral hemodynamics and metabolism in human adults. *NeuroImage* 12, 623–639.
- Ogawa, S., Tank, D., Menon, R., Ellermann, J., Kim, S.-G., Merkle, H., Ugurbil, K., 1992. Intrinsic signal changes accompanying sensory stimulation: functional brain mapping with magnetic resonance imaging. *Proc. Natl. Acad. Sci.* 89, 5951–5955.
- Okada, F., Tokumitsu, Y., Hoshi, Y., Tamura, M., 1994. Impaired interhemispheric integration in brain oxygenation and hemodynamics in schizophrenia. *Eur. Arch. Psychiatry Clin. Neurosci.* 244, 17–25.
- Okada, E., Schweiger, M., Arridge, S.R., Firbank, M., Delpy, D.T., 1996. Experimental validation of Monte Carlo and finite-element methods of estimation of the optical path length in inhomogeneous tissue. *Appl. Opt.* 35, 3362–3371.
- Okada, F., Takahashi, N., Tokumitsu, Y., 1996. Dominance of the 'nondominant' hemisphere in depression. *J. Affect Disord.* 37, 13–21.
- Okada, E., Firbank, M., Schweiger, M., Arridge, S.R., Cope, M., Delpy, D.T., 1997. Theoretical and experimental investigation of near-infrared light propagation in a model of the adult head. *Appl. Opt.* 36, 21–31.
- O'Leary, M.A., Boas, D.A., Chance, B., Yodh, A.G., 1995. Experimental images of heterogeneous turbid media by frequency-domain diffusing-photon tomography. *Opt. Lett.* 20, 426–428.
- Patterson, M.S., Chance, B., Wilson, B.C., 1989. Time resolved reflectance and transmittance for the non-invasive measurement of tissue optical properties. *Appl. Opt.* 28, 2331–2336.
- Paulsen, K.D., Jiang, H., 1995. Spatially varying optical property reconstruction using a finite element diffusion equation approximation. *Med. Phys.* 22, 691–701.
- Pena, M., Maki, A., Kovacic, D., Dehaene-Lambertz, G., Koizumi, H., Bouquet, F., Mehler, J., 2003. Sounds and silence: an optical topography study of language recognition at birth. *Proc. Natl. Acad. Sci. U. S. A.* 100, 11702–11705.
- Pogue, B.W., Paulsen, K.D., 1998. High-resolution near-infrared tomographic imaging simulations of the rat cranium by use of a priori magnetic resonance imaging structural information. *Opt. Lett.* 23, 1716–1718.
- Prince, S., Kolehmainen, V., Kaipio, J.P., Franceschini, M.A., Boas, D., Arridge, S.R., 2003. Time-series estimation of biological factors in optical diffusion tomography. *Phys. Med. Biol.* 48, 1491–1504.
- Ruben, J., Wenzel, R., Obrig, H., Villringer, K., Bernarding, J., Hirth, C., Hecker, H., Dirnagl, U., Villringer, A., 1997. Haemoglobin oxygenation changes during visual stimulation in the occipital cortex. *Adv. Exp. Med. Biol.* 428, 181–187.
- Saitou, H., Yanagi, H., Hara, S., Tsuchiya, S., Tomura, S., 2000. Cerebral blood volume and oxygenation among poststroke hemiplegic patients: effects of 13 rehabilitation tasks measured by near-infrared spectroscopy. *Arch. Phys. Med. Rehabil.* 81, 1348–1356.
- Sakatani, K., Chen, S., Lichty, W., Zuo, H., Wang, Y.P., 1999. Cerebral blood oxygenation changes induced by auditory stimulation in newborn infants measured by near infrared spectroscopy. *Early Hum. Dev.* 55, 229–236.
- Sato, H., Takeuchi, T., Sakai, K.L., 1999. Temporal cortex activation during speech recognition: an optical topography study. *Cognition* 73, B55–B66.
- Sato, H., Kiguchi, M., Kawaguchi, F., Maki, A., 2004. Practicality of wavelength selection to improve signal-to-noise ratio in near-infrared spectroscopy. *NeuroImage* 21, 1554–1562.
- Schotland, J.C., 1997. Continuous-wave diffusion imaging. *J. Opt. Soc. Am.* 14, 275–279.
- Schotland, J.C., Haselgrove, J.C., Leigh, J.S., 1993. Photon hitting density. *Appl. Opt.* 32, 448–453.
- Siegel, A.M., Marota, J.J., Boas, A., 1999. Design and evaluation of a continuous-wave diffuse optical tomography system. *Opt. Express* 4, 287–298.
- Siegel, A.M., Culver, J.P., Mandeville, J.B., Boas, D.A., 2003. Temporal comparison of functional brain imaging with diffuse optical tomography and fMRI during rat forepaw stimulation. *Phys. Med. Biol.* 48, 1391–1403.
- Sokol, D.K., Markand, O.N., Daly, E.C., Luerssen, T.G., Malkoff, M.D., 2000. Near infrared spectroscopy (NIRS) distinguishes seizure types. *Seizure* 9, 323–327.
- Steinbrink, J., Kohl, M., Obrig, H., Curio, G., Syre, F., Thomas, F., Wabnitz, H., Rinneberg, H., Villringer, A., 2000. Somatosensory evoked fast optical intensity changes detected non-invasively in the adult human head. *Neurosci. Lett.* 291, 105–108.
- Steinbrink, J., Wabnitz, H., Obrig, H., Villringer, A., Rinneberg, H., 2001. Determining changes in NIR absorption using a layered model of the human head. *Phys. Med. Biol.* 46, 879–896.
- Steinhoff, B.J., Herrendorf, G., Kurth, C., 1996. Ictal near infrared spectroscopy in temporal lobe epilepsy: a pilot study. *Seizure* 5, 97–101.
- Strangman, G., Culver, J.P., Thompson, J.H., Boas, D.A., 2002. A quantitative comparison of simultaneous BOLD fMRI and NIRS recordings during functional brain activation. *NeuroImage* 17, 719–731.
- Strangman, G., Franceschini, M.A., Boas, D.A., 2003. Factors affecting the accuracy of near-infrared spectroscopy concentration calculations for focal changes in oxygenation parameters. *NeuroImage* 18, 865–879.
- Thirion, B., Fugères, O., 2003. Dynamical components analysis of fMRI data through kernel PCA. *NeuroImage* 20, 34–49.
- Toronov, V., Franceschini, M.A., Filiaci, M., Fantini, S., Wolf, M., Michalos, A., Gratton, E., 2000. Near-infrared study of fluctuations in cerebral hemodynamics during rest and motor stimulation: temporal analysis and spatial mapping. *Med. Phys.* 27, 801–815.

- Toronov, V., Webb, A., Choi, J.H., Wolf, M., Michalos, A., Gratton, E., Hueber, D., 2001. Investigation of human brain hemodynamics by simultaneous near-infrared spectroscopy and functional magnetic resonance imaging. *Med. Phys.* 28, 521–527.
- Torricelli, A., Pifferi, A., Taroni, P., Giambattistelli, E., Cubeddu, R., 2001. In vivo optical characterization of human tissues from 610 to 1010 nm by time-resolved reflectance spectroscopy. *Phys. Med. Biol.* 46, 2227–2237.
- Uludag, K., Kohl, M., Steinbrink, J., Obrig, H., Villringer, A., 2002. Cross talk in the Lambert-Beer calculation for near-infrared wavelengths estimated by Monte Carlo simulations. *J. Biomed. Opt.* 7, 51–59.
- Vernieri, F., Rosato, N., Pauri, F., Tibuzzi, F., Passarelli, F., Rossini, P.M., 1999. Near infrared spectroscopy and transcranial Doppler in monohemispheric stroke. *Eur. Neurol.* 41, 159–162.
- Walker, S.A., Fantini, S., Gratton, E., 1997. Image reconstruction by backprojection from frequency-domain optical measurements in highly scattering media. *Appl. Opt.* 36, 170–179.
- Wang, L., Jacques, S.L., Zheng, L., 1995. MCML—Monte Carlo modeling of light transport in multi-layered tissues. *Comput. Methods Programs Biomed.* 47, 131–146.
- Watanabe, E., Maki, A., Kawaguchi, F., Yamashita, Y., Koizumi, H., Mayanagi, Y., 2000. Noninvasive cerebral blood volume measurement during seizures using multichannel near infrared spectroscopic topography. *J. Biomed. Opt.* 5, 287–290.
- Wobst, P., Wenzel, R., Kohl, M., Obrig, H., Villringer, A., 2001. Linear aspects of changes in deoxygenated hemoglobin concentration and cytochrome oxidase oxidation during brain activation. *NeuroImage* 13, 520–530.
- Wolf, M., Wolf, U., Toronov, V., Michalos, A., Paunescu, L.A., Choi, J.H., Gratton, E., 2002. Different time evolution of oxyhemoglobin and deoxyhemoglobin concentration changes in the visual and motor cortices during functional stimulation: a near-infrared spectroscopy study. *NeuroImage* 16, 704–712.
- Wray, S., Cope, M., Delpy, D.T., 1988. Characteristics of the near infrared absorption spectra of cytochrome aa3 and hemoglobin for the non-invasive monitoring of cerebral oxygenation. *Biochim. Biophys. Acta* 933, 184–192.
- Yamashita, Y., Maki, A., Koizumi, H., 2001. Wavelength dependence of the precision of noninvasive optical measurement of oxy-, deoxy-, and total-hemoglobin concentration. *Med. Phys.* 28, 1108–1114.
- Yao, Y., Wang, Y., Pei, Y., Zhu, W., Barbour, R.L., 1997. Frequency-domain optical imaging of absorption and scattering distributions using a born iterative method. *JOSA A* 14, 325–342.
- Zhang, Y., Brooks, D.H., Franceschini, M.A., Boas, D.A., 2004. Eigenvector-based spatial filtering for reduction of physiological interference in diffuse optical imaging. *J. Biomed. Opt.* (in press).
- Zourabian, A., Siegel, A., Chance, B., Ramanujan, N., Rode, M., Boas, D.A., 2000. Trans-abdominal monitoring of fetal arterial blood oxygenation using pulse oximetry. *J. Biomed. Opt.* 5, 391–405.